Supporting Information for:

$Cu_{3-x}P$ Nanocrystals as a Material Platform for Plasmonics and Cation Exchange Reactions

Luca De Trizio,[1] Roberto Gaspari,[2] Giovanni Bertoni,[1,8] Ilka Kriegel,[3,4] Luca Moretti,[3,4] Francesco Scotognella,[3,4] Lorenzo Maserati,[1] Yang Zhang,[1] Gabriele C. Messina,[5] Mirko Prato,[1] Sergio Marras,[1] Andrea Cavalli[6,7] and Liberato Manna[1]*

[1] Department of Nanochemistry, Istituto Italiano di Tecnologia (IIT), via Morego, 30, 16163 Genova, Italy

[2] CONCEPT Lab, Istituto Italiano di Tecnologia (IIT), via Morego, 30, 16163 Genova, Italy

[3] Department of Physics, Politecnico di Milano, Piazza L. Da Vinci 32, 20133 Milano, Italy

[4]Center for Nano Science and Technology@PoliMi, Istituto Italiano di Tecnologia (IIT), Via Giovanni Pascoli 70/3, 20133 Milan, Italy

[5] Department of Nanostructures, Istituto Italiano di Tecnologia (IIT), via Morego, 30, 16163 Genova, Italy

[6]CompuNet, Istituto Italiano di Tecnologia (IIT), via Morego, 30, 16163 Genova, Italy

[7]Dept. of Pharmacy and Biotechnology, University of Bologna, via Belmeloro 6, I-40126, Italy

[8]IMEM-CNR, Parco Area delle Scienze 37/A, 43124 Parma, Italy

Computational Details

a) Computational setup

Cu vacancy formation energies in $Cu_{3-x}P$ were computed using the Kohn-Sham formulation[1] of density functional theory[2] (KS-DFT). All calculations were performed using the PWSCF package.[3] Ultrasoft pseudopotentials[4] were employed for Cu and P atoms[5,6] in all systems. The KS wave functions and charge density were expanded in plane waves, using respectively a 30 Ryd and 240 Ryd cutoff. Structural optimization was stopped at a force threshold of $1 \cdot 10^{-4}$ Ry/Bohr. The PBE functional[7] was used. All copper phosphide systems that were simulated consisted of one periodically repeated unit cell (starting from 18 Cu and 6 P atoms/unit cell for systems displaying no vacancies). K-point sampling was achieved using a 5x5x5 Monkhorst-Pack grid.[8] Bulk copper was simulated in the *fcc* orthorhombic unit cell (4 at/unit cell) using a 8x8x8 Monkhorst-Pack grid. Bulk phosphorous was simulated in the low temperature beta form of the white phase[9] (24 at/unit cell). The structurally important dispersive interactions between phosphorous atoms were accounted for by the use of the Grimme D2[10] correction. Grimme D2 corrections were also applied to bulk Cu and Cu_3P only for the calculation of the Cu_3P formation enthalpy (see section "Calculation of vacancy formation energies" later in the SI for further details). A 5x5x5 Monkhorst-Pack was used. Optimal lattice parameters were found to be a=7.04 Å and *c*=7.32 Å for hexagonal stoichiometric Cu_3P, and *a*=3.67 Å for cubic copper. For the beta form of phosphorous, the triclinic cell was scaled by the same factor on all the lattice directions, which yielded an optimal lattice parameter a=11.27 Å.

Calculations of the bond-order in Cu_3P were performed according to the methods described by Angyan et al.[11] (see also SI for further details). The electron charge density and the occupied electron states of stoichiometric Cu_3P, required by the Bader[12,13] and the bond orders analysis, were computed using CP2K.[14] The unit cell employed was a 2x2x2 model of the primitive unit cell.

Calculations were performed at the Γ point of the Brillouin zone. We used double zeta valence basis sets with polarization for Cu and P atoms.[15] Goedecker-Teter-Hutter pseudopotentials[16] were used. The charge density was expanded in plane waves using a cutoff of 400 Hartree and the system was structurally optimized up to a force threshold of $1 \cdot 10^{-4}$ Hartree/Bohr.

b) Estimation of the bond order and charge transfer in Cu_3P

We used the Bader scheme for the partitioning of the charge density into individual atomic contributions, by employing the implementation presented by Tang *et al.*.[13] The use of such partitioning allows for the definition of atomic volumes as regions delimited by surfaces where the flux of the charge density gradient vanishes. The integral of the electron density over one particular basin represents a measure of the charge on the atom associated with the basin. Consequently this defines the amount of charge transfer occurring between individual atoms. The Bader partitioning can also be used to estimate the bond order between two neighboring atoms. By labeling, for instance, a reference atoms as A, it is possible to define an overlap matrix S_{ij} referred to A as:

$$S_{ij}(A) = \int_{\Omega(A)} \psi_i^* \psi_j dr \qquad (1)$$

where Ω(A) is the volume associated with the basin A while ψ_i and ψ_j represents two occupied Kohn-Sham states. The sum

$$B_{AB} = \sum_{ij} S_{ij}(A) S_{ij}(B) \qquad (2)$$

represents the bond order between atom A and B as defined in the work of Angyan *et al.*.[11] The bond order calculation has been performed on the unit composed of 1 P atom surrounded by 11 Cu coordinated atoms. The results for the P-Cu and Cu-Cu bonds of the unit are presented in Figure S1

.

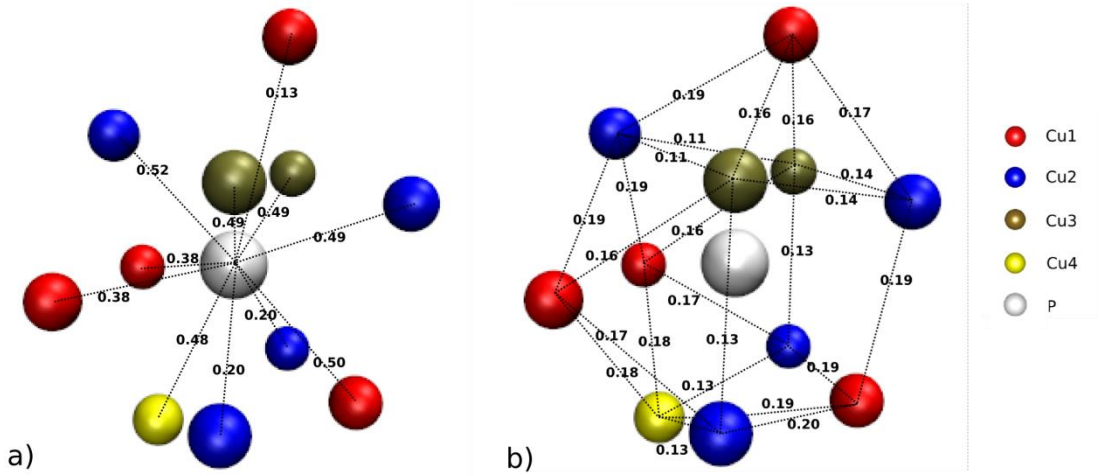

Figure S1. *Structure of the atomic unit containing one P atom coordinated to 11 Cu atoms. Neighboring P-Cu (a) and Cu-Cu (b) atom pairs are connected with a dotted line. The number associated with each bond represents the bond order.*

c) Calculation of vacancy formation energies

The formation energy of one single Cu vacancy $E_v(1)$ in the Cu_3P primitive unit cell was computed for all possible Cu sites as:

$$E_v(1) = E_N - E_{N-1} - \mu_{Cu} \qquad (3)$$

where μ_{Cu} is the chemical potential of copper, E_N (N = 24) is the energy of the bulk with no vacancies, and E_{N-1} is the DFT energy of the bulk with one Cu vacancy. Similarly, we also computed the formation energies of one additional vacancy in systems containing already one or two vacancies. Such formation energies, $E_v(2)$ and $E_v(3)$, are given as:

$$E_v(x) = E(min)_{N-x+1} - E_{N-x} - \mu_{Cu} \qquad (4)$$

x being either 2 or 3 and $E(min)_{N-x}$ representing the lowest energy system containing x vacancies. The range of allowed μ_{Cu} is given by the thermodynamic stability of Cu_3P[17] and can be expressed as:

$$\frac{n_{Cu}\mu_{Cu(bulk)} + \Delta H_f}{n_{Cu}} \leq \mu_{Cu} \leq \mu_{Cu(bulk)} \qquad (5)$$

where ΔH_f is the enthalpy of formation of Cu_3P, $n_{Cu} = 18$ is the total number of copper atoms in bulk stoichiometric Cu_3P and $\mu_{Cu(bulk)}$ is the energy required to extract one copper atom from bulk elemental copper. The meaning of Eq. 5 can be understood as follows: on one hand the right inequality states that μ_{Cu} must be smaller than $\mu_{Cu(bulk)}$ otherwise copper in Cu_3P would precipitate into elemental bulk copper; similarly, using standard thermodynamic considerations[17], it can be shown that the left inequality implies that μ_P must be smaller than $\mu_{P(bulk)}$. At the boundaries of the stability range, Cu_3P is in equilibrium with bulk Cu (Cu-rich) and bulk P (P-rich). When this happens, crystallites of Cu and P coexist with the Cu_3P sample. The enthalpy of formation of Cu_3P was calculated as:

$$\Delta H_f = E_N - n_{Cu}\mu_{Cu(bulk)} - n_P\mu_{P(bulk)} \qquad (6)$$

where in our case $\mu_{P(bulk)}$ =1/24 $E_{P(bulk)}$, $E_{P(bulk)}$ being the DFT energy of one bulk of white phosphorous. Grimme corrections have been used on all systems only for the calculations of Cu_3P formation enthalpy. In this way the level of theory employed is the same in the calculations of all terms in Eq. (6) allowing for the removal of possible systematic errors in calculating the energy differences. Using Grimme corrections a set of optimized lattice paramaters are obtained for bulk Cu (3.61 Å) and Cu_3P (a=c=7.02 Å). Since the most stable DFT structure of Cu_3P actually contains one copper vacancy over the largest part of the chemical potential stability range (see the Results section in the main text), we also computed the ΔH_f of that system and we found that the difference with respect to the stoichiometric case is less than 10 meV. Even if the energy stability range is very narrow (142 meV) this difference does not change our conclusions on Cu_3P in P-rich conditions. In this aspect, we also note that while the Cu-rich boundary of the stability phase diagram is well defined, owing to the unique crystal structure of bulk copper, the P-rich boundary is more difficult to be described, partly because of the problematic treatment of dispersive interactions in DFT, and partly because of the large number of allotropes of bulk phosphorous. Actually the P-rich boundary of the Cu_3P stability range depends on the phase chosen for the calculations on bulk phosphorous.

This cannot be strictly controlled and might depend on experimental conditions. In our case, the choice of the common white beta phase provides an estimation of the lower bound of μ_{Cu}. The consistency between the predicted and experimental stoichiometry at P-rich conditions (see the Results section in the main text) appears however to corroborate the estimation made. Actual values of the vacancy formation energies as expressed by Eq. (4) are reported in Table S1, together with optimized positions of the lowest energy systems displaying 0, 1 and 2 vacancies.

Site	Coordinates (0 vacancies)			$E_v(1)$	Coordinates (1 vacancy)			$E_v(2)$	Coordinates (2 vacancies)			$E_v(3)$
Cu1	0,729	0,729	0,078		0,71	0,722	0,077	209	0,707	0,724	0,078	372
Cu1	0,27	0	0,078		0,289	0,011	0,077	209	0,3	0	0,079	629
Cu1	0	0,27	0,078	-117	V1				V1			
Cu1	0,729	0	0,578		0,728	-0,013	0,578	127	0,711	-0,012	0,578	367
Cu1	0	0,729	0,578		0	0,727	0,576	133	0,014	0,742	0,573	367
Cu1	0,27	0,27	0,578		0,271	0,257	0,578	131	0,271	0,242	0,571	335
Cu2	0,384	0	0,426	-99	0,382	-0,013	0,427	116	V2			
Cu2	0	0,384	0,426		0	0,365	0,421	397	-0,002	0,364	0,421	567
Cu2	0,615	0,615	0,426		0,617	0,603	0,427	116	0,617	0,603	0,43	324
Cu2	0,615	0	0,926		0,665	0,06	0,927	223	0,68	0,075	0,933	313
Cu2	0	0,615	0,926		0	0,618	0,923	191	-0,015	0,607	0,923	360
Cu2	0,384	0,384	0,926		0,334	0,395	0,927	223	0,345	0,391	0,923	384
Cu3	0,333	0,666	0,189	162	0,332	0,666	0,206	447	0,331	0,664	0,222	640
Cu3	0,666	0,333	0,689		0,668	0,333	0,678	317	0,668	0,335	0,678	629
Cu3	0,333	0,666	0,689		0,331	0,665	0,678	317	0,328	0,662	0,208	308
Cu3	0,666	0,333	0,189		0,667	0,333	0,206	447	0,667	0,335	0,208	629
Cu4	0	0	0,327	54	0	-0,002	0,836	395	-0,004	0	0,303	626
Cu4	0	0	0,827		0	-0,002	0,754	296	0,002	-0,002	0,836	417
P1	0,33	0	0,751		0,334	-0,003	0,754		0,34	-0,003	0,749	
P1	0	0,33	0,751		0	0,327	0,756		0,003	0,326	0,754	
P1	0,669	0,669	0,751		0,665	0,661	0,754		0,668	0,666	0,753	
P1	0,669	0	0,251		0,674	0,005	0,247		0,658	0	0,252	
P1	0	0,669	0,251		0	0,665	0,249		0	0,668	0,249	
P1	0,33	0,33	0,251		0,325	0,331	0,247		0,325	0,327	0,246	

Table S1. *DFT-optimized coordinates for the system displaying 0,1,2 Cu vacancies, respectively. $E_v(1)$ is reported for four, arbitrarily chosen, non-equivalent Cu sites. V1 is the predicted most stable single vacancy in the system. Starting from the system containing V1, the energy $E_v(2)$ of adding a second vacancy is computed for all possible Cu sites. This defines the second most stable vacant site V2. Starting from the system containing V1 and V2 the formation energy of a third vacancy, $E_v(3)$, is computed. All vacancy formation energies are reported at Cu-rich conditions ($\mu_{Cu} = \mu_{Cu\ (bulk)}$). The lowest $E_v(1)$ and $E_v(2)$ are highlighted in red.*

d) Estimation of the temperature dependence of the vacancy density

We estimate the effect of temperature on the average number of vacancies by using Boltzmann statistics. We employ a very simple model, with the only aim to observe the qualitative behavior of the Cu_3P copper content in the temperature range employed int the $Cu_3P \rightarrow InP$ cation exchange process. Taking into account the experimental homogeneity range of Cu_3P, we consider a model Cu_3P as composed only of subsystems containing one or two Cu vacancies per unit cell. These subsystems should be large enough so that the energy penalty due to the interface between them can be disregarded. This assumption is necessary since we will now associate with these subsystems the energy obtained by calculations on periodic infinite Cu_3P bulk systems, displaying either one or two vacancies per unit cell. We take only one bulk system containing a single Cu vacancy per unit cell, i.e. the one corresponding to the lowest energy and to the Cu1 vacant site. The energy of this system, $E_v(1)$, for this calculation is set to 0. The bulk systems containing two vacancies per unit cell and which are included in the model correspond to those described in Table S1. Their energy, relative to $E_v(1)$, is reported in Table S1 and is expressed as $E_v(2)^n$. The superscript n represents the specific two-vacancy bulk system considered and ranges from 1 to 17. The grand canonical partition function of the mixture of subsystems with one or two vacancies is given as:

$$Z = 1 + \sum_n e^{-\beta E_v(2)^n} \qquad (7)$$

where $\beta = 1/kT$, k is the Boltzmann constant, and T is the temperature. The dependency on μ_{Cu} is implicit in the definition of $E_v(x)$ given in Eq. (4). The average number of vacancies <n> per unit cell can be computed using standard statistical mechanics considerations as:

$$< n > = \left(1 + 2\sum_n e^{-\beta E_v(2)^n}\right)/Z \qquad (8)$$

A plot of the average number of vacancies per unit cell as a function of the temperature and copper chemical potential is shown in Figure S2.

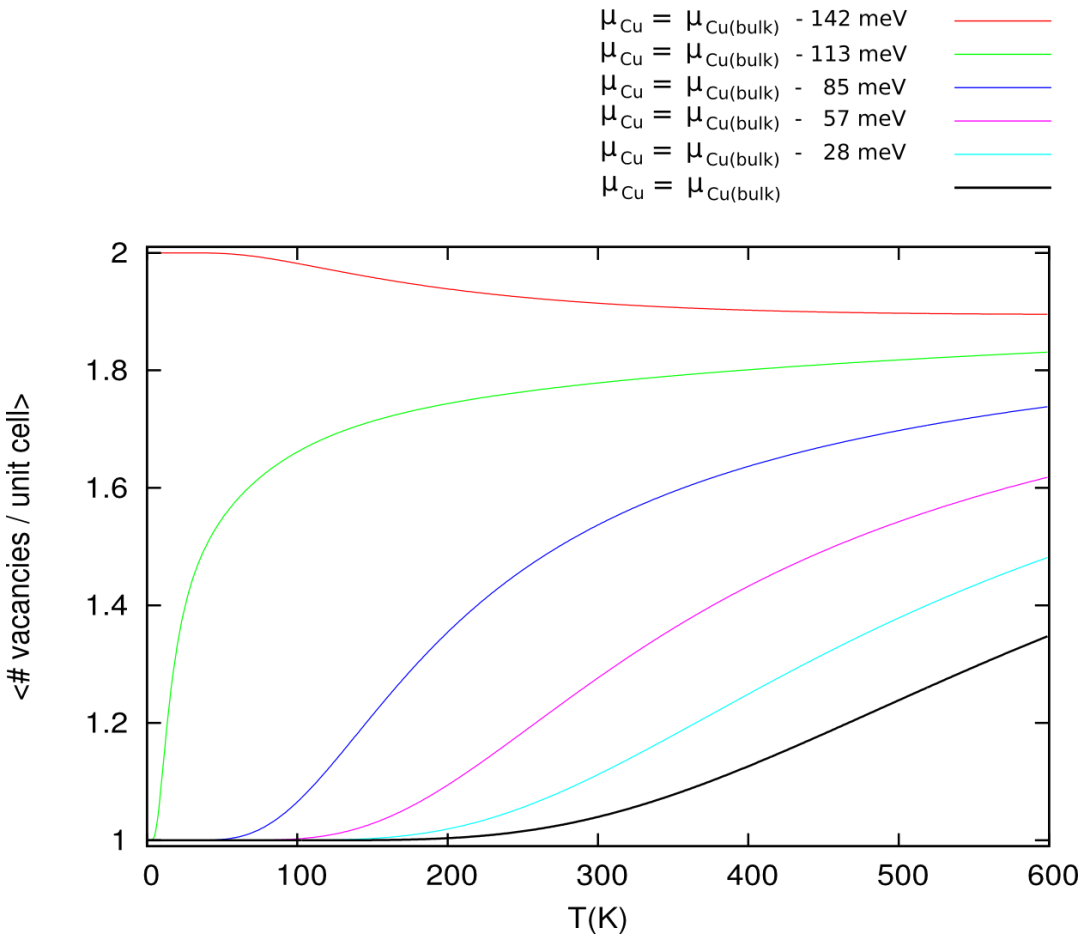

Figure S2. *Average number of vacancies per unit cell as a function of the temperature and the copper chemical potential.*

e) DFT band structure

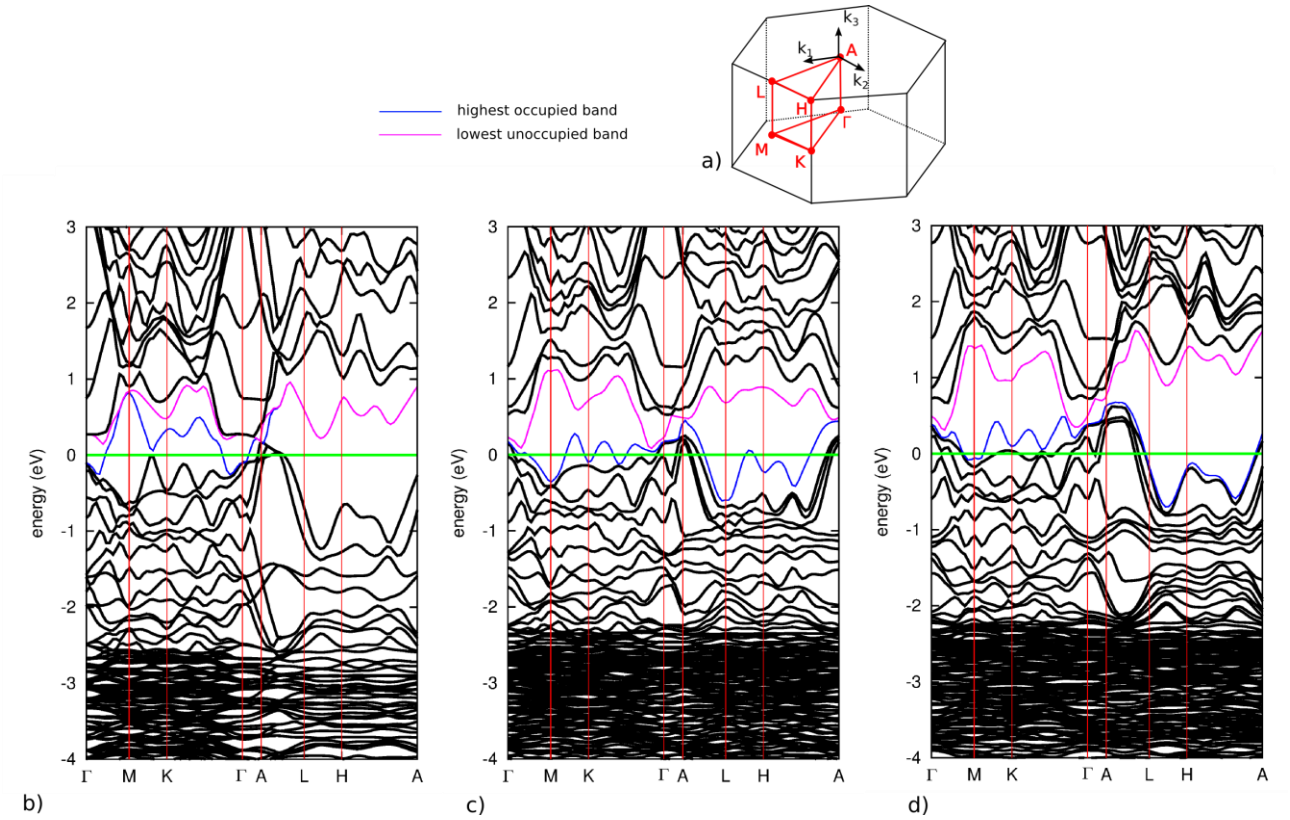

Figure S3. *Band structure along the high symmetry lines of the hexagonal Brillouin zone (a) of Cu_3P: (b) stoichiometric Cu_3P, (c) lowest energy Cu_3P system with one vacancy, (d) lowest energy Cu_3P system with two vacancies. The highest occupied and lowest unoccupied bands are displayed. Note that along the L-H-A line these two bands become degenerate in the case of stoichiometric Cu_3P, this degeneracy disappears by the introduction of Cu vacancies.*

Thermo-electrical measurements

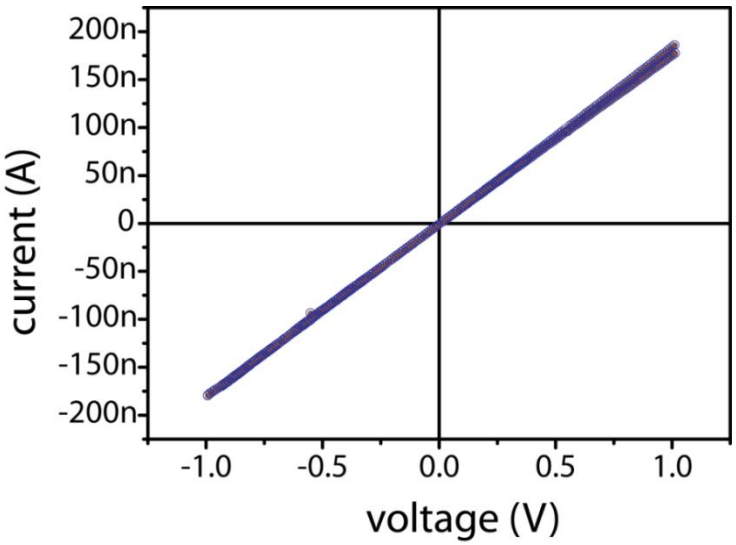

Figure S4. *Two loops of current-voltage curves measured across two Au pads deposited on a* $Cu_{3-x}P$ *NCs film. The linear behavior of these curves clearly indicates that ohmic contacts were formed between the Au pads and the NCs film.*

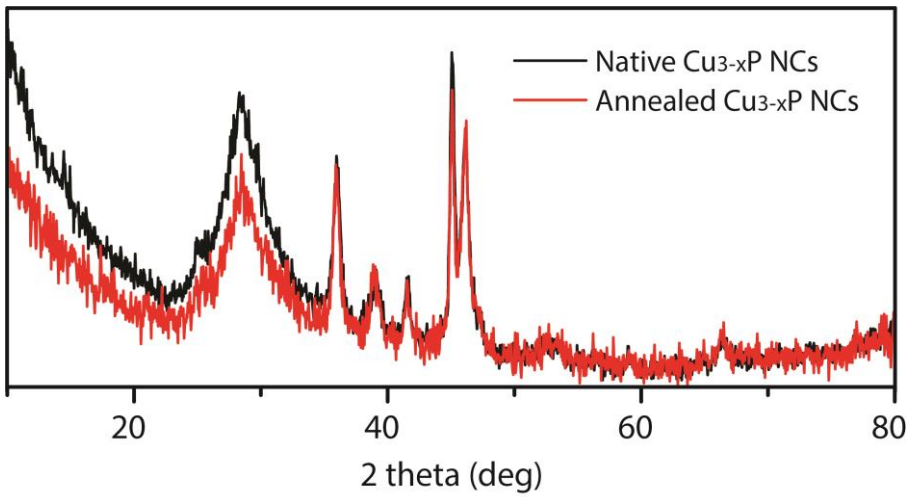

Figure S5. *X-ray diffraction patterns obtained from a dropcast solution of* $Cu_{3-x}P$ *NCs before and after an annealing process at 200°C under inert atmosphere. The organic ligands are responsible for the scattering at low angle and for the wide peak at about 28°. As it is possible to see from the collected XRD patterns the annealing process reduces the scattering at low angle and thus the amount of residual organic in the film. At the same time it does not cause any alteration of the hexagonal* $Cu_{3-x}P$ *phase peaks implying no structural modification of the NCs.*

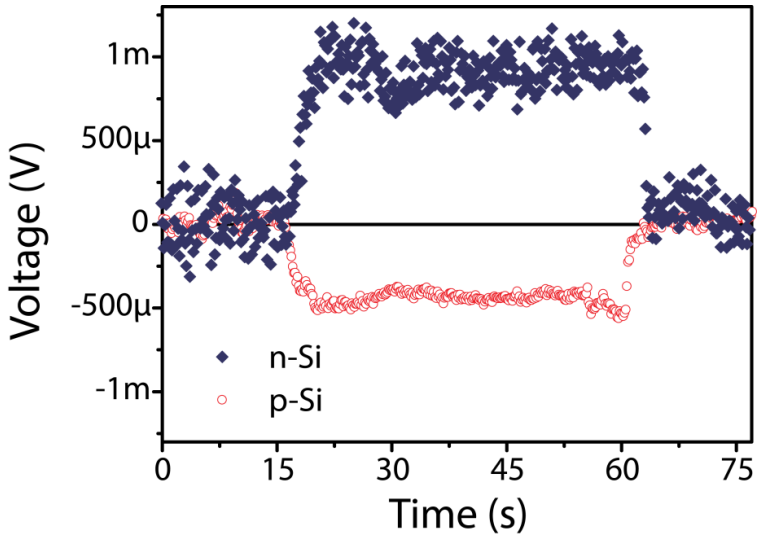

Figure S6. *Hot-probe thermoelectric measurements on p-type (red circles) and n-type (blue diamonds) silicon wafers using the same experimental configuration as sketched in Figure 2a in the main text. The conductivity type of the silicon wafers is known from the specification provided by the supplier. It can be seen that, the positive and negative values of the thermoelectric voltage are associated with n-type and p-type conduction, respectively. These measurements are used as a calibration for our experimental setup.*

X-ray Photoelectron Spectroscopy (XPS) analysis

XPS analysis was performed on the native $Cu_{3-x}P$ NCs and on a NCs film used for the thermo-electrical measurements, after the annealing treatment at 200°C under inert atmosphere. In both cases the samples preparation was performed in a N_2-filled glovebox and the so-obtained specimens were then transferred into the XPS setup avoiding air exposure. XPS analyses confirmed the presence of a $Cu_{3-x}P$ phase constituted of Cu^+ ions and P^{3-} anions without any presence of Cu^{2+} species. In fact, as shown in Figure S7, there is no trace of Cu(II) satellites at approx. 940 eV in the Cu 2p spectrum. Moreover, the position of the Cu $2p_{3/2}$ peak at binding energy of (932.8 ± 0.2) eV, together with the position of the Cu LMM Auger peak at kinetic energy of (917.8 ± 0.2) eV indicates the presence of Cu(I) species.[18]

The P 2p signal is composed of two components: the narrow doublet, characterized by a P $2p_{3/2}$ peak at (128.9 ± 0.2) eV, that can be attributed to P^{3-} species[2] and a broad peak at approximately 133eV, that can be assigned to TOP molecules bound to the surface. It is interesting to note that after the annealing process performed for the thermo-electrical measurements the Cu^{+} and P^{3-} signals were unaffected while the intensity of the peak at 133eV was reduced, suggesting again a decrease of the organic phase.

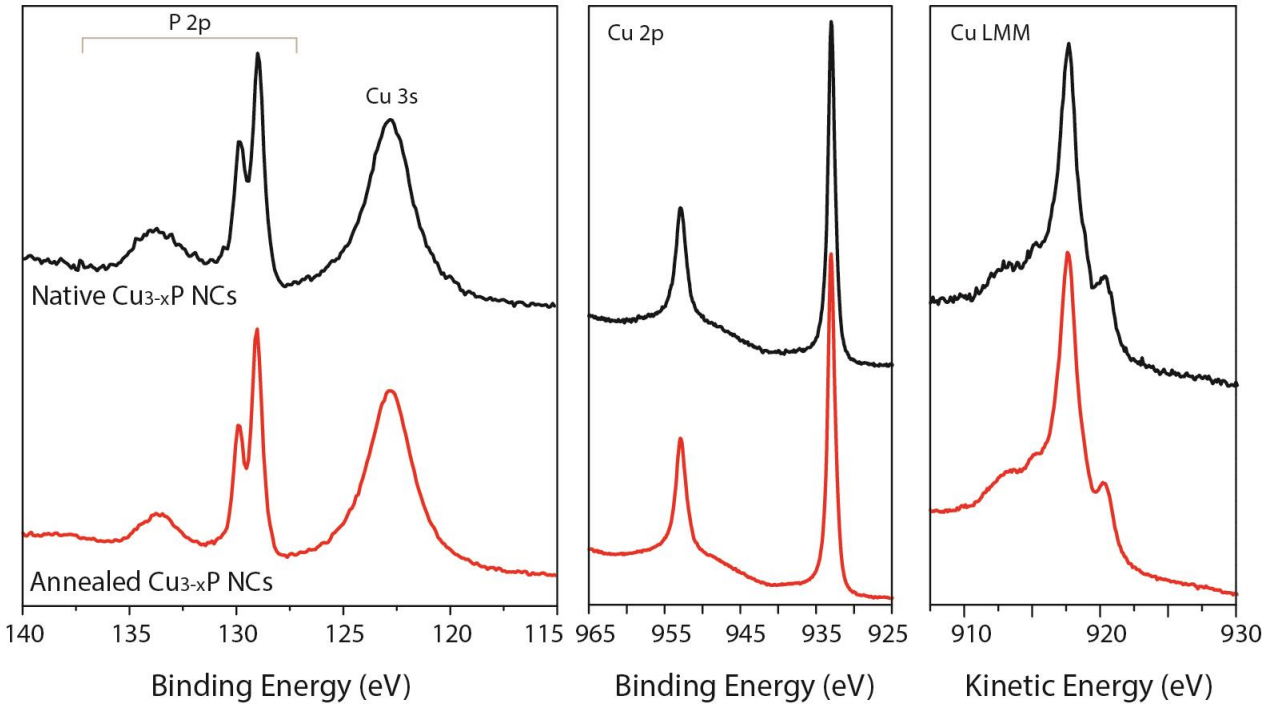

Figure S7. *High resolution XPS spectra of the $Cu_{3-x}P$ NCs before (black curves) and after (red curves) the annealing process at 200°C under inert atmosphere in the region of the Cu 3s and P 2p peaks (left panel), Cu 2p peaks (middle panel) and Cu LMM Auger peak (right panel).*

Refinement of the structural parameters of Cu_3P nanocrystals with the FP method

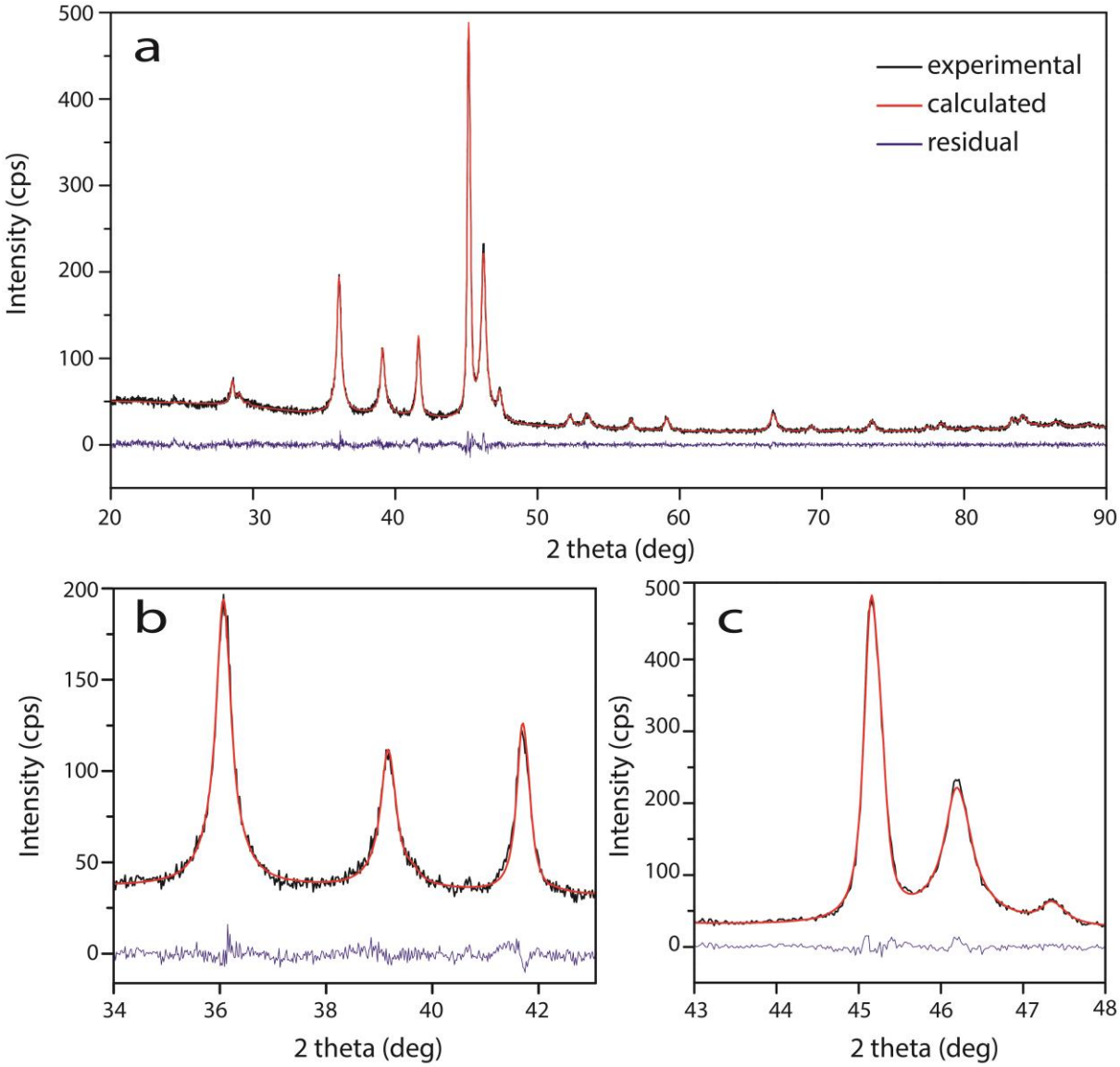

***Figure S8**. (a) The refined XRD profile of $Cu_{3-x}P$ NCs using the FP method with a zoom over the (b) 34°-43° and (c) 43°-48° 2-theta range. In each panel the red curve represents the calculated profile and the black one the experimental data; also, on the bottom, the difference profile between experimental and calculated curves is reported. Figures of the refinement are R_{wp}=5.73% and S=1.010, where R_{wp} is the weighted profile R-factor and S is the goodness of fit.*

Energy Dispersive X-ray Spectroscopy (EDXS) analysis on the obtained InP WZ NCs

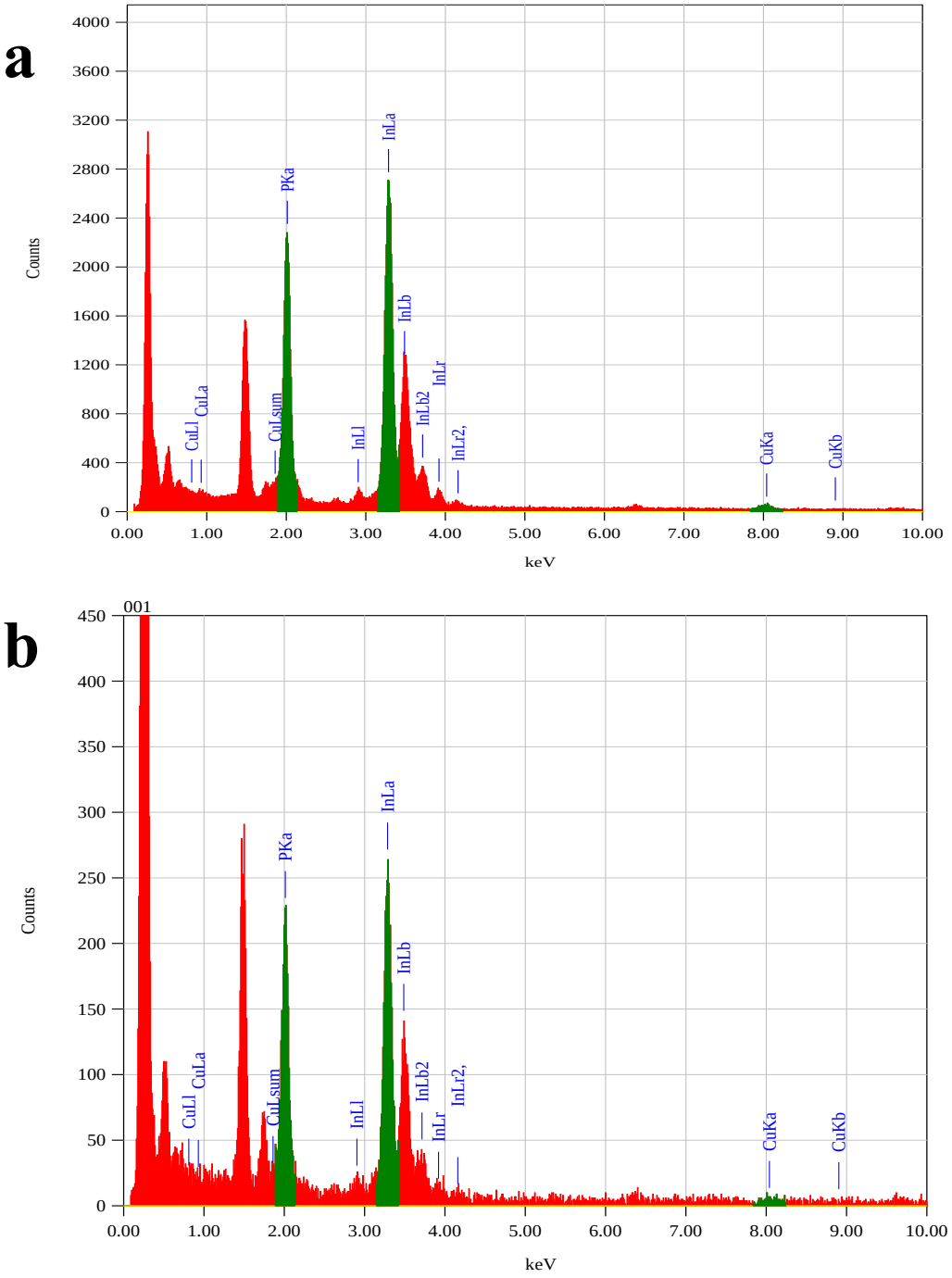

Figure S9. *EDXS analysis on (a) several InP NCs, and (b) single InP NC. The calculated atomic percentages in both cases are: P=42%, In=57%, Cu=1%.*

Partial cation exchange experiments

In the partial cation exchange synthesis a sub-stoichiometric amount of In^{3+} in respect to Cu^{+} ions was used. A solution of $InBr_3$ (0.01mmol), TOP (1.5ml), and ODE (3.5ml) was degassed at 130°C for 1h and then heated up to 200°C. At this point a solution of $Cu_{3-x}P$ NCs in degassed ODE (1ml), containing 0.06mmol of Cu^{+} ions (that is a In:Cu molar ratio of 1:6), was added to the reaction flask and the solution was allowed to react for 15 minutes at 200°C. The residual amount of copper in this experiment is about 54% (the Cu:In molar ratio found by ICP is 1.16) .

HAADF-STEM, HRTEM images and the elemental maps of some $Cu_{3-x}P$/InP heterostructures obtained starting from large (~100nm) $Cu_{3-x}P$ NCs are presented in Figure S10.

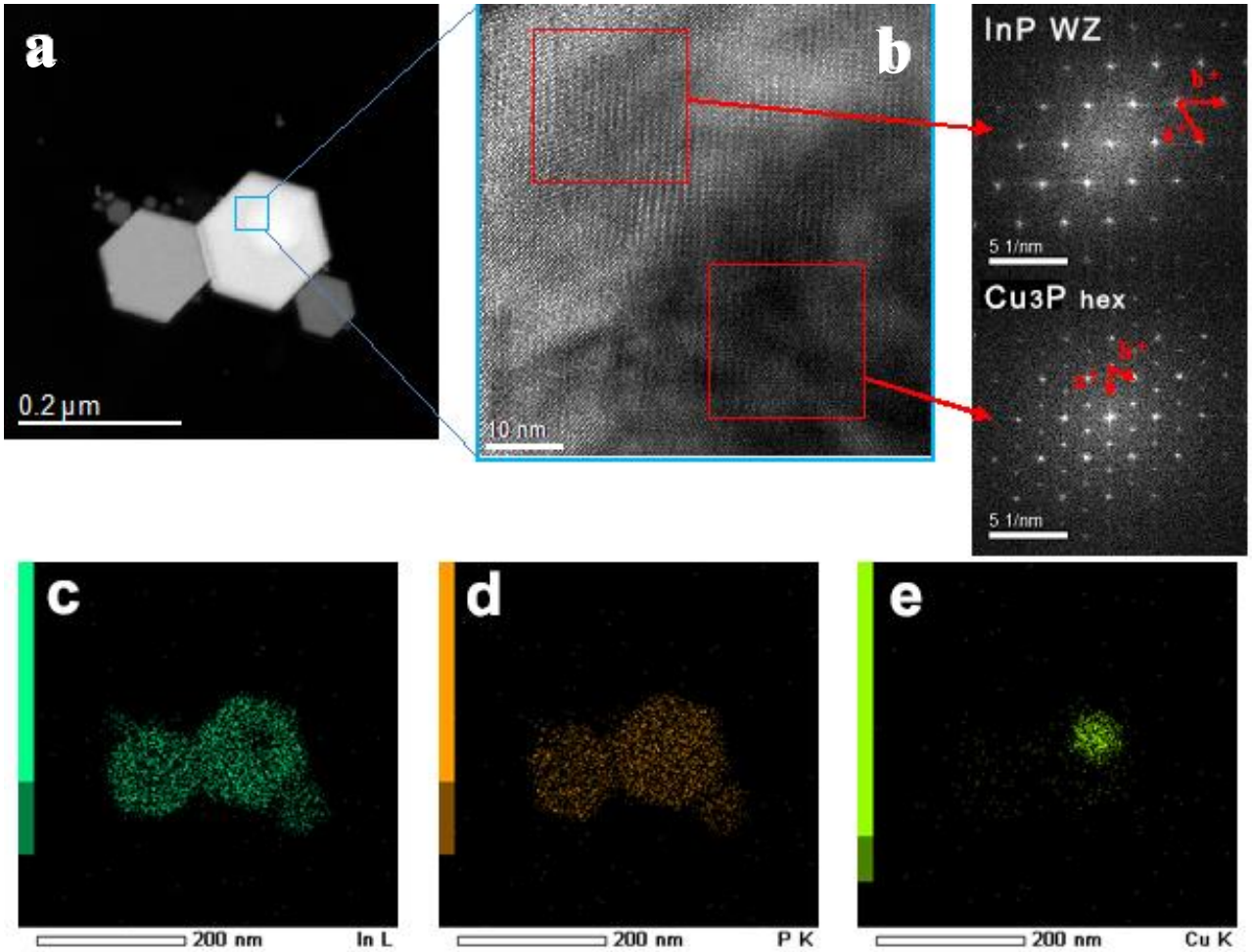

***Figure S10**. (a) HAADF-STEM image of a partially exchanged $Cu_{3-x}P$/InP NC (central platelet) and some totally exchanged InP NCs. (b) Detail of the Cu_3P/InP interface in a heterostructured NC. From the FFT of the two different domains the 30° orientation relationship between Cu_3P and InP structures can be clearly visualized. The red arrows indicate the reciprocal lattice vectors. The NC is sufficiently thick to see the (100) reflections of Cu_3P. (c-e) EDXS elemental maps for In, P, and Cu, respectively. The elemental maps confirm the depletion of Cu ions from the native NCs and their replacement by In cations, except for the core region of the central platelet.*

Cation exchange experiment using TBP

A solution of $InBr_3$ (0.5 mmol), TBP (1.5 ml), and ODE (3.5 ml) was degassed at 130°C for 1h and then heated to 200°C. At this point a solution of $Cu_{3-x}P$ NCs in degassed ODE (1 ml), containing 0.2 mmol of Cu atoms (that is a In:Cu molar ratio of 1:1), was added to the reaction flask and the solution was allowed to react for 15 minutes at 200°C. The NCs were washed twice by dissolution in chloroform followed by precipitation upon addition of ethanol. The resulting NCs showed a 10:1 copper to indium ratio, measured by ICP elemental analysis, suggesting that a very poor exchange occurred in this experiment.

Additional References

(1) Hohenberg, P. *Physical Review* **1964**, *136*, B864.

(2) Kohn, W.; Sham, L. J. *Physical Review* **1965**, *140*, A1133.

(3) Giannozzi, P.; Baroni, S.; Bonini, N.; Calandra, M.; Car, R.; Cavazzoni, C.; Ceresoli, D.; Chiarotti, G. L.; Cococcioni, M.; Dabo, I.; Dal Corso, A.; de Gironcoli, S.; Fabris, S.; Fratesi, G.; Gebauer, R.; Gerstmann, U.; Gougoussis, C.; Kokalj, A.; Lazzeri, M.; Martin-Samos, L.; Marzari, N.; Mauri, F.; Mazzarello, R.; Paolini, S.; Pasquarello, A.; Paulatto, L.; Sbraccia, C.; Scandolo, S.; Sclauzero, G.; Seitsonen, A. P.; Smogunov, A.; Umari, P.; Wentzcovitch, R. M. *Journal of physics. Condensed matter : an Institute of Physics journal* **2009**, *21*, 395502.

(4) Vanderbilt, D. *Physical Review B* **1990**, *41*, 7892.

(5) P.pbe-mt_fhi.UPF and Cu.pbe-mt_fhi.UPF from http://www.quantum-espresso.org.

(6) P.pbe-n-rrkjus psl.0.1.UPF and Cu.pbe-d-rrkjus.UPF from http://www.quantum-espresso.org.

(7) Perdew, J. P.; Burke, K.; Ernzerhof, M. *Phys Rev Lett* **1996**, *77*, 3865.

(8) Monkhorst, H. J.; Pack, J. D. *Physical Review B* **1976**, *13*, 5188.

(9) Simon, A.; Borrmann, H.; Craubner, H. *Phosphorus and Sulfur and the Related Elements* **1987**, *30*, 507.

(10) Wedeking, K.; Mu, Z. C.; Kehr, G.; Sierra, J. C.; Lichtenfeld, C. M.; Grimme, S.; Erker, G.; Frohlich, R.; Chi, L. F.; Wang, W. C.; Zhong, D. Y.; Fuchs, H. *Chem-Eur J* **2006**, *12*, 1618.

(11) Angyan, J. G.; Loos, M.; Mayer, I. *The Journal of Physical Chemistry* **1994**, *98*, 5244.

(12) Bader, R. F. W. *Atoms in Molecules: a Quantum Theory*; Oxford University Press: New York, 1990.

(13) Tang, W.; Sanville, E.; Henkelman, G. *Journal of Physics: Condensed matter* **2009**, *21*.

(14) VandeVondele, J.; Krack, M.; Mohamed, F.; Parrinello, M.; Chassaing, T.; Hutter, J. *Computer Physics Communications* **2005**, *167*, 103.

(15) VandeVondele, J.; Hutter, J. *The Journal of Chemical Physics* **2007**, *127*, 114105.

(16) Goedecker, S.; Teter, M.; Hutter, J. *Physical Review B* **1996**, *54*, 1703.

(17) Qian, G.-X.; Martin, R. M.; Chadi, D. J. *Physical Review B* **1988**, *38*, 7649.

(18) Moulder, J. F.; Stickle, W. F.; Sobol, P. E.; Bomben, K. D. *Handbook of X-ray photoelectron spectroscopy*; Perkin Elmer Eden Prairie, MN, 1992; Vol. 40.